Magnetism in multiferroic Pb5Cr3F19

Blinc, Robert; Cevc, Pavel; Tavčar, Gašper; Žemva, Boris; Laguta, Valentin; Trontelj, Zvonko; Jagodič, Marko; Pajić, Damir; Balčytis, Armandas; Scott, James F.

Repository / Repozitorij:

Repository of the Faculty of Science - University of Zagreb

Magnetism in multiferroic $Pb_5Cr_3F_{19}$

Robert Blinc,[1,*] Pavel Cevc,[1] Gašper Tavčar,[1] Boris Žemva,[1] Valentin Laguta,[2] Zvonko Trontelj,[3,†] Marko Jagodič,[3]
Damir Pajić,[4] Armandas Balčytis,[5] and James F. Scott[6]

[1]*Jožef Stefan Institute, Ljubljana, Slovenia*
[2]*Institute of Physics AS CR, Prague, Czech Republic*
[3]*Institute of Mathematics, Physics and Mechanics, Ljubljana, Slovenia*
[4]*Department of Physics, Faculty of Science, University of Zagreb, Bijenička c. 32, 10000 Zagreb, Croatia*
[5]*Vilnius University, Vilnius, Lithuania*
[6]*Cavendish Laboratory, Department of Physics, Cambridge University, Cambridge, United Kingdom*
(Received 17 August 2011; revised manuscript received 30 December 2011; published 16 February 2012)

We report on the first observation of a magnetic transition in multiferroic $Pb_5Cr_3F_{19}$. The system undergoes a ferroelectric transition at $T_C = 545$ K and probably an antiferromagnetic transition around $T_N = 11$ K. Between 50 K and T_N, the system is not paramagnetic but shows the presence of correlated spin clusters, indicating a superparamagnetic or spin glass state. The observable changes of the magnetic properties ongoing through ferroelectric phase transition show a magnetoelectric coupling that may be important for new devices.

I. INTRODUCTION

Multiferroic systems, and in particular magnetoelectrics, in which magnetism and ferroelectricity coexist have many potential applications in spintronics as electrically switchable magnets and as new kinds of memory devices. However, the coexistence of magnetism and ferroelectricity in oxides is unlikely, because according to Nicola Hill-Spaldin, ferromagnetism requires a d^n electronic configuration with a nonzero n, whereas ferroelectricity requires a d^0 orbital.[1,2] In view of that, there is an intensive search for new families of multiferroics and ferroelectrics that are not based on oxide perovskites.[3]

Ravez showed that the $Pb_5(Cr,Ti,V,Fe)_3F_{19}$ family contains 4 multiferroic isomorphs with ferroelectric Curie temperatures $T_C = 545$ K (Cr), 695 K (Ti), 630 K (V), and 740 K (Fe).[4] If Sr or Ba is substituted for Pb, the number of multiferroic compounds in this family is increased to 12. However, magnetism has not yet been found in this family of materials.

It is the purpose of this paper to present a study of the magnetic properties of $Pb_5Cr_3F_{19}$ as obtained by electron paramagnetic resonance (EPR) and superconducting quantum interference device (SQUID) magnetic measurements. Preliminary results of this study were presented briefly in our last review paper.[5]

$Pb_5Cr_3F_{19}$ is characterized at 295 K by the tetragonal $I4cm$ space group with $a = 14.384(5)$ Å and $c = 7.408(2)$ Å.[6,7] The structure consists of chains of CrF_6 octahedra and chains of PbF_4 tetrahedra running along the c axis connected through $[CrFPbFPbF]$ six-membered rings (Fig. 1).[5,6] There are two crystallographically nonequivalent Cr sites in the ferroelectric phase. The two symmetry-independent Cr atoms are displaced from the paraelectric mirror plane, in opposite directions, by 0.22 Å. This allows for relative atomic displacements of the fluorine octahedra about each Cr atom. The effective displacement Δz of these atoms is 0.19 Å for Cr(1) and 0.18 Å for Cr(2).[6]

The a lattice constant of tetragonal $Pb_5Cr_3F_{19}$ expands by 0.6% on heating through the Curie temperature ($T_c = 545$ K). In contrast, the c lattice constant abruptly contracts by 0.6%.[7]

No larger $Pb_5Cr_3F_{19}$ single crystals were available to us. The ferroelectric phase transition has been deduced from dielectric measurements on ceramic samples.[7] Dielectric measurements on ceramic samples of $Pb_5Cr_3F_{19}$ showed a T_c of 580 K on heating and 530 K on cooling, demonstrating the first-order nature of the phase transition. The same effect is seen in the thermal hysteresis of the optical birefringence.[7] The average entropy change (ΔS) at the transition is 13 J mol^{-1} K^{-1}.[7]

In the isomorphous $Pb_5Al_3F_{19}$, the Al shifts are parallel in the ferroelectric phase and antiparallel in the antiferroelectric phase, whereas the Al ions sit in the centers of the octahedra in the ferroelastic phase.[6]

II. EXPERIMENTAL DETAILS

All manipulations were carried out in an inert atmosphere of argon. Polycrystalline $Pb_5Cr_3F_{19}$ was prepared by the reaction between 0.513 g (4.706 mmol) CrF_3 (Alfa Aesar, 99.9%) and 1.924 g (7.847 mmol) PbF_2 (Merck, Suprapur) in 3:5 molar ratio. The reaction mixture was put in a gold reaction vessel, sealed, and heated for 48 h at 800 K, as described previously.[7] The green product was characterized by x-ray single crystal diffraction and Raman spectroscopy and is in accordance with the published structure.[6]

Single crystal data sets were collected using a Mercury charge-coupled device area detector coupled to a Rigaku AFC7 diffractometer using graphite monochromated Mo-Kα radiation ($\lambda = 0.71069$ Å). Raman spectra of samples were recorded on a Renishaw Raman Imaging Microscope System 1000 by use of the 632.8-nm exciting line of a He-Ne laser. Geometry for all Raman experiments was 180° backscattering with laser power of 25 mW. The X-band and the Q-band EPR spectra were taken by a Bruker Elexsys E-850 spectrometer. Temperature dependence of magnetization $M(T)$ and magnetic hysteresis loops $M(H)$ were measured using a Quantum Design MPMS-XL-5 SQUID magnetometer. $M(T)$ was measured in the 100-Oe field after it was zero-field cooled (ZFC) and field cooled (FC).
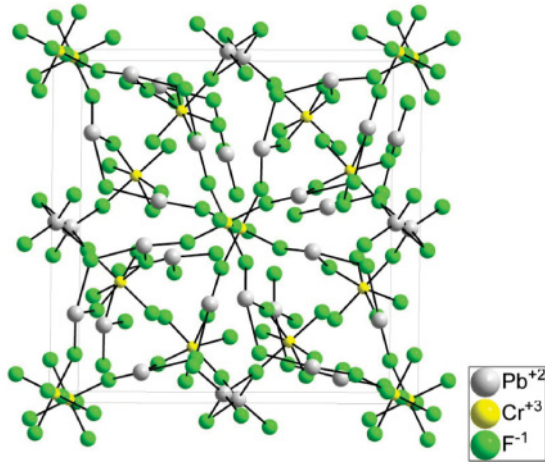
FIG. 1. (Color online) Crystal structure of $Pb_5Cr_3F_{19}$ (Ref. [5]).

III. RESULTS AND DISCUSSION

A. High-temperature EPR spectra

The X-band $\frac{\omega_L}{2\pi} = 9.57$ GHz EPR spectra of polycrystalline $Pb_5Cr_3F_{19}$ at 295, 532, 545, and 602 K are presented in Fig. 2(a). The spectra consist of a narrow central component, which can be approximately described by a Lorentzian line shape. Because $Pb_5Cr_3F_{19}$ contains paramagnetic Cr^{3+} ions, the measured EPR spectra are surely produced by these ions that have an electron spin of 3/2.

The temperature dependences of the g-factor, the line width δH—determined as the full width at half maximum (FWHM)—are shown in Fig. 3. The g-factor, which measures the position of the EPR line, is nearly T−independent up to $T_c = 545$ K, where it shows on heating a discontinuous increase from $g_{\mathrm{ferro}} = 1.978$ to $g_{\mathrm{para}} = 2.003$. A similar discontinuous increase is seen in the EPR line width that increases on heating through T_c from 52 to 110 mT. Above T_c, it is practically T-independent.

The Q-band spectra at 295 K show an increase in line width from 51.8 mT in the X-band to 68.4 mT in the Q-band. This seems to be the result of the two slightly nonequivalent Cr^{3+} sites in the unit cell.

To estimate the line width due to dipolar interactions between nearest-neighbor Cr^{3+} ions, we used the Anderson-Weiss approach.[8] The FWHM at the infinitive temperature is given by

$$\Delta B_d = \left(5.1 \frac{g^4 \beta^4}{h^2} S(S+1) \frac{1}{d^6}\right)^{1/2}, \tag{1}$$

where d is the Cr^{3+}–Cr^{3+} nearest-neighbor distance, g is the g-factor, and β and h are the Bohr magneton and the Planck constant, respectively. By taking $d = 3.7$ Å, $g = 1.97$, and $S = 3/2$, we obtain $\Delta B_d \approx 3600$ Oe. This is three times larger than the measured line width at $T > 550$ K. Therefore, the Cr^{3+} EPR line is exchange narrowed. This is supported by its quasi-Lorentzian shape.

In general, the temperature dependence of FWHM (ΔB) of the exchange-narrowed EPR line can be written as[9,10]

$$\Delta B = \Delta B_0 (T\chi_0)^{-1} \Gamma(T), \tag{2}$$
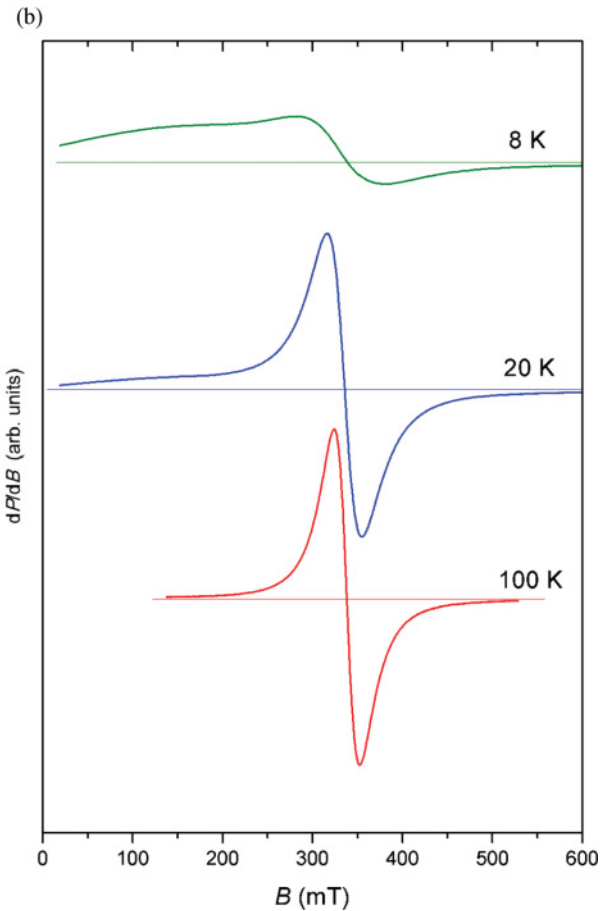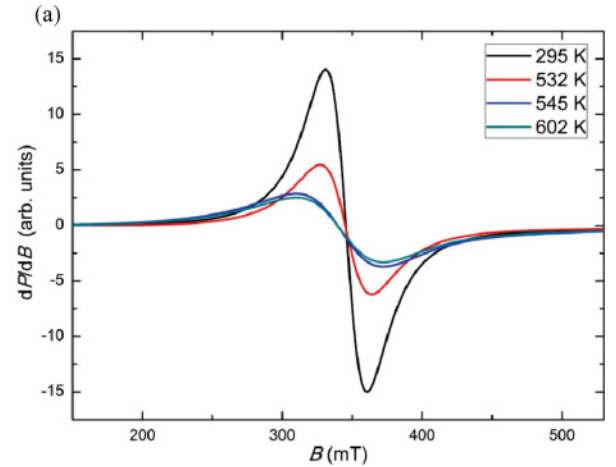

FIG. 2. (Color online) (a) High-temperature X-band EPR spectra of $Pb_5Cr_3F_{19}$ and (b) low-temperature X-band EPR spectra. The horizontal "zero amplitude line" in (b) helps us see the EPR line asymmetry and the appearance of a new broad line below 20 K.

where χ_0 is the static susceptibility and $\Gamma(T)$ is a kinetic coefficient that depends on dynamic spin–spin correlations. The line width ΔB_0 is given by the well-known expression[8]

$$\Delta B_0 = \frac{2\omega_d^2}{\gamma \omega_{\mathrm{ex}}}, \tag{3}$$

where ω_d is the dipolar width in frequency units and ω_{ex} is the exchange frequency. Both can be obtained from moment

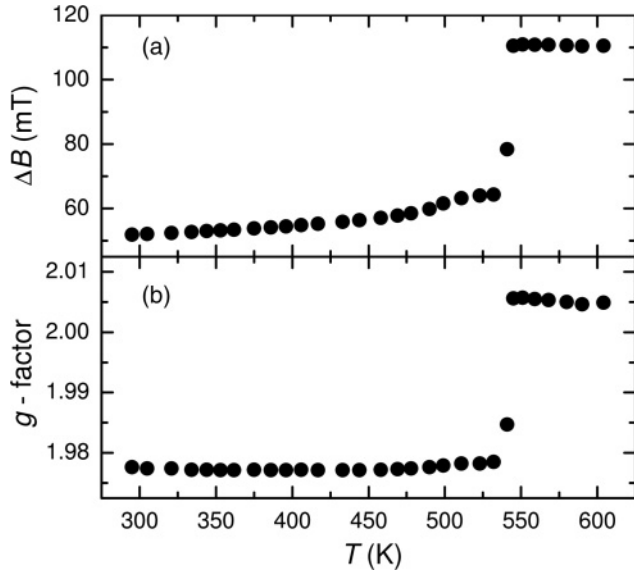FIG. 3. Temperature dependence of the (a) EPR line width and (b) g-factor in Pb$_5$Cr$_3$F$_{19}$ close to the ferroelectric transition.

method calculations [Eq. (1)].[8] It is reasonable to assume that the $\Gamma(T)$ function is T-independent at $T \gg T_0$, where T_0 is the temperature of the magnetic phase transition. In this case, the
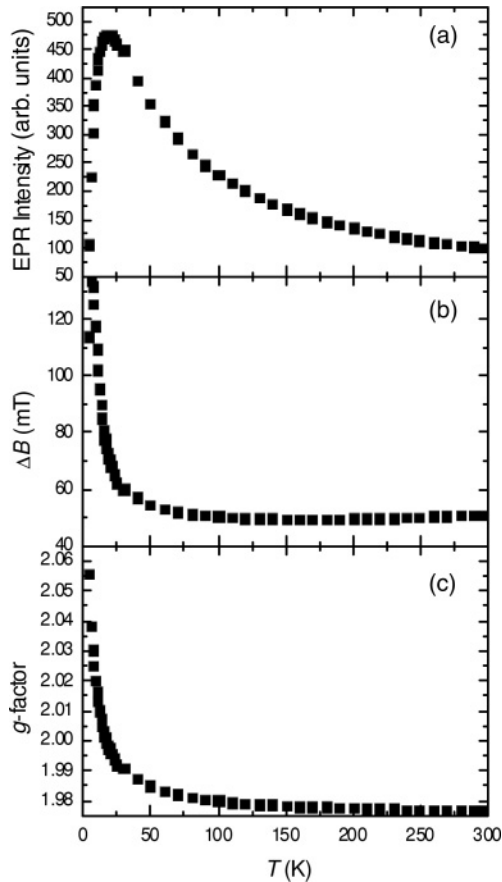

FIG. 4. Temperature dependence of the (a) EPR intensity, (b) line width, and (c) g-factor of the central line below room temperature.
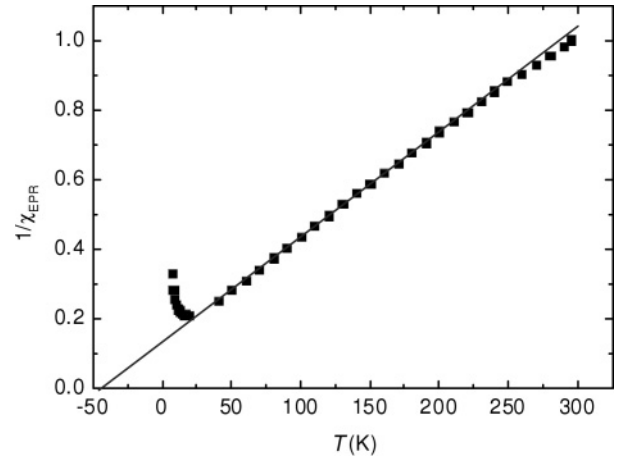

FIG. 5. Inverse EPR susceptibility versus temperature for the central line.

Curie-Weiss behavior of the high-temperature susceptibility should result in a line width that has the following dependence:

$$\Delta B(T) = \Delta B_0 \left(1 + \frac{T_0}{T}\right), \qquad (4)$$

where T_0 is the Curie-Weiss temperature. At $T \gg T_0$, the line width should be T-independent, as we indeed observed (Fig. 3).

The exchange frequency can be obtained from Eq. (3). It is $\sim 5 \times 10^{10}$ Hz, which corresponds to the exchange energy of 1.6 cm^{-1}. At temperatures below 540 K, the line width drops to ~ 50 mT. This is accompanied by a change in the g-factor (Fig. 3). The changes of the spectral parameters of Cr^{3+} are due to the ferroelectric phase transition. This leads to a modification of both magnetic dipole–dipole and exchange interactions. The changes may be, to a great extent, due to the contraction of the c lattice constant and the expansion of the a lattice constant ongoing through the ferroelectric transition. The dielectric constant data show that this transition is of the first order. In our opinion, most changes come from the exchange interaction between the Cr^{3+} ions. This is very sensitive to the coordination of all ions, not only paramagnetic ones. From structural data, it is well known that not only the
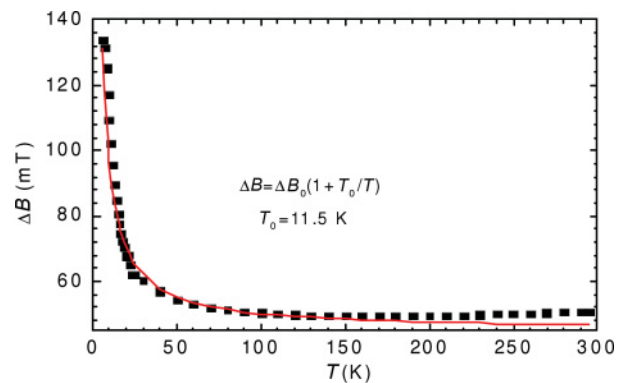

FIG. 6. (Color online) Cr^{3+} EPR line broadening as a function of temperature for the central line. The solid line is the fit of the experimental data to Eq. (4).
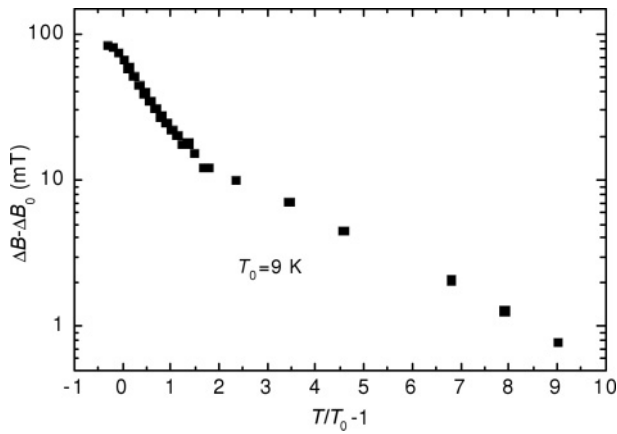
FIG. 7. Excess line width as a function of $T/T_0 - 1$.

FIG. 9. Temperature dependence of $\chi \cdot T$ as obtained from ZFC SQUID magnetic susceptibility data of $Pb_5Cr_3F_{19}$ at $H = 100$ Oe. The inset shows $\Delta\chi$ versus $(T_c - T)$.

Cr position but also the Pb^{2+} and the fluorine atom positions change at T_c. By using the same dipole–dipole line width as in the paraelectric phase, the line width in the ferroelectric phase at $T < 530$ K can be described by the exchange frequency 1.5×10^{11} Hz, which corresponds to the exchange energy 5 cm^{-1} or 7 K.

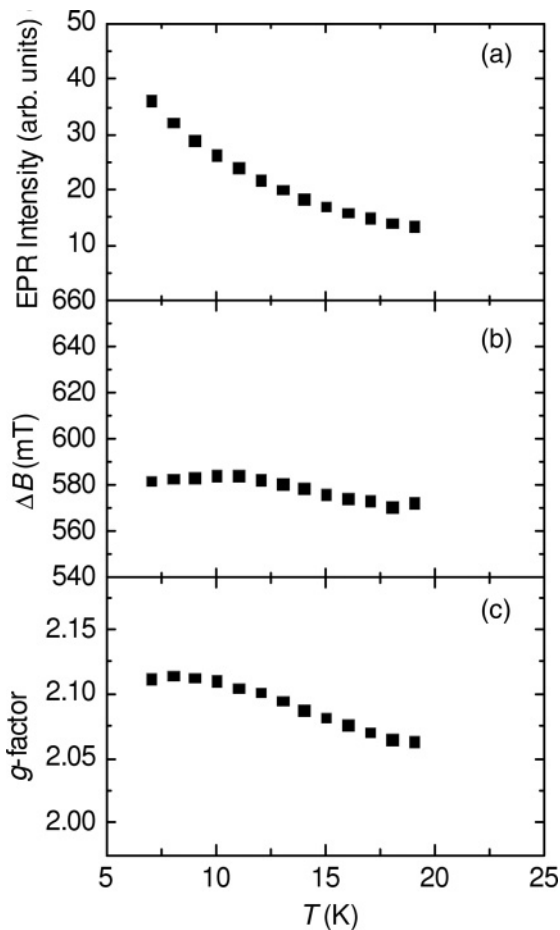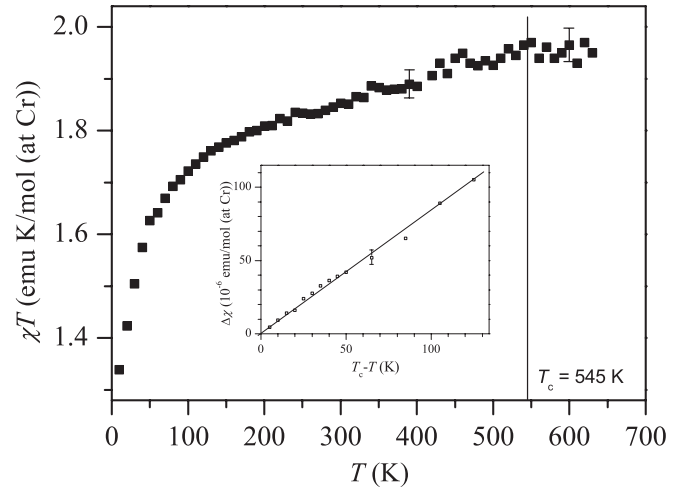The noticeable changes in the magnetic properties at the ferroelectric transition show strong coupling among the

electric, structural, and magnetic degrees of freedom. The coupling between the polarization and the magnetization here is probably quadratic. That can also be seen from the linear dependence of the $\Delta\chi$ versus $(T_c - T)$ graph shown as the inset to Fig. 9. In that inset, $\Delta\chi$ is the difference between the static magnetic susceptibility in the paraelectric phase (which is practically a constant value) and the susceptibility in the ferroelectric phase below T_c.[11] Measurements at higher temperatures are more difficult, and a larger error bar is shown in Fig. 9 and in the Fig. 9 inset.

B. Low-temperature spectra

The X-band EPR spectra measured at $T = 100$, 20, and 8 K are presented in Fig. 2(b). The temperature dependence of the EPR intensity, line width, and g-factor (below room temperature) are in Fig. 4. The critical broadening of the EPR line and maximum in EPR intensity and the later decrease

FIG. 8. Temperature dependence of the (a) EPR line intensity, (b) line width, and (c) g-factor for the broad line in $Pb_5Cr_3F_{19}$ at low temperatures.
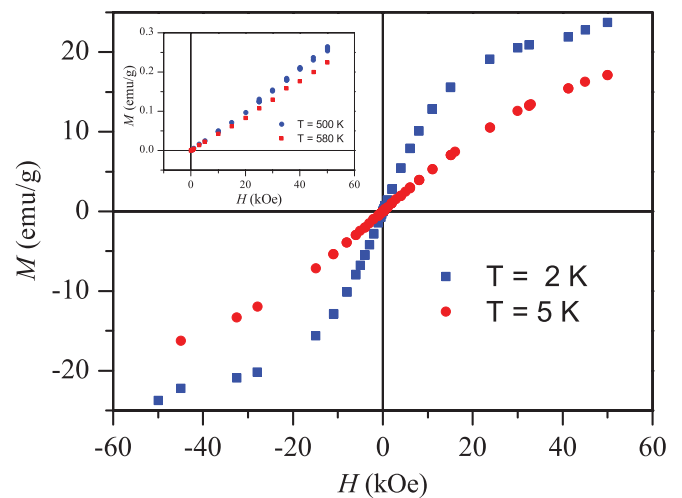

FIG. 10. (Color online) Magnetization as a function of the magnetic field at $T = 2$ and 5 K. The inset shows M versus H at $T = 500$ and 580 K.

at $T < 20$ K are typical for an antiferromagnetic transition. This is further supported by the temperature dependence of the inverse susceptibility $1/\chi_{EPR}$ as shown in Fig. 5. Between 300 and 25 K, the plot is linear, and it goes to zero at -50 K. This shows that we are probably dealing with an antiferromagnetic type of transition. (For a paraelectric system the plot should go to zero at $T = 0$, whereas for a ferromagnetic system it should go to zero at a positive temperature.)

The static susceptibility times the temperature, or $\chi \cdot T$, versus the temperature T shows a large decrease below 25 K, characteristic of a magnetic phase transition (Fig. 9).

The Cr^{3+} EPR line broadening as a function of temperature from $\sim$200 K down to 11 K can be approximately fitted with Eq. (4) (solid line in Fig. 6), with $T_0 = 11.5$ K and $\Delta B_0 = 45$ mT. This shows that the magnetic transition temperature is $\sim$11 K.

Often, the critical broadening of the EPR line in magnetic systems can be analyzed as a function of $T/T_0 - 1$, giving $T_0 = 9$ K. This is shown for the excess line width in Fig. 7, which shows two regions: above 20 K and below 20 K. Below 20 K, the slope is different and the excess line width seems to be dominated by critical spin fluctuations and their freezing $\sim$11 K with the onset of some order between Cr^{3+} spins.

Below 20 K, an additional broad line appears [Fig. 2(b)]. The temperature dependence of the EPR line intensity, line width, and g-factor below 20 K are shown in Fig. 8. It may well be that this is part of an antiferromagnetic resonance line. Only part of it can be seen, because we are dealing with polycrystalline powder.

C. SQUID data

The temperature dependence (from 10 to 630 K) of the ZFC magnetic susceptibility times the temperature of Pb$_5$Cr$_3$F$_{19}$ measured by a SQUID magnetometer at $H = 100$ Oe is shown in Fig. 9. The FC and ZFC susceptibilities are identical. The results of SQUID magnetometer measurements are practically the same as the EPR ones, thus confirming the validity of our approach. The magnetization as a function of the magnetic field up to 50 kOe was measured at $T = 2, 5, 500,$ and 580 K, i.e., below the magnetic transition in the low-temperature region and above the ferroelectric transition in the high-temperature region. It is shown in Fig. 10. The important point is that no magnetic hysteresis loops exist, thus excluding ferromagnetic, ferrimagnetic, or spin glass order.

IV. CONCLUSIONS

The Cr^{3+} ($S = 3/2$) EPR spectra of Pb$_5$Cr$_3$F$_{19}$ are exchange narrowed, because the observed X-band and Q-band widths of the central line ($\sim$50–100 mT) is much smaller than the expected dipolar width ($\sim$360 mT). The exchange frequency is on the order of 10^{11} Hz, which corresponds to the exchange energy 5 cm^{-1}.

There are two large anomalies in the EPR spectra: at the ferroelectric transition $T_C = 545$ K and at the magnetic transition around $T_N \approx 11$ K. The behavior of the EPR intensity, line width, and g-factor shows that the magnetic transition is probably an antiferromagnetic one. This is supported by SQUID magnetization data. The SQUID magnetization measurements below T_N show that no magnetic hysteresis loops should be present for a ferromagnet, a weak ferrimagnet, or a spin glass state. In addition, between T_C and T_N, the EPR line width is not T-independent as expected for an ordinary paramagnet but is continuously increasing with decreasing temperature. The behavior seems to show the presence of correlated spin clusters reminiscent of a superparamagnetic or spin glass state between T_N and 50 K.

*Deceased.

†zvonko.trontelj@fmf.uni-lj.si

[1] N. A. Hill, J. Phys. Chem. B **104**, 6694 (2000).

[2] R. E. Cohen and H. Krakauer, Ferroelectrics **136**, 95 (1992).

[3] R. Blinc, P. Cevc, A. Potočnik, B. Žemva, E. Goreshnik, D. Hanžel, A. Gregorovič, Z. Trontelj, Z. Jagličič, M. Perović, N. Dalal, and J. F. Scott, J. Appl. Phys. **107**, 043511 (2010).

[4] J. Ravez, Comptes Rend. Ser. II **3**, 267 (2000); J. Ravez, J. Phys. III **8**, 1129 (1997); J. Ravez, S. Arquis, and J. Grannec, J. Appl. Phys. **62**, 4299 (1987).

[5] J. F. Scott and R. Blinc, J. Phys. Condens. Matter **23**, 113202 (2011).

[6] S. C. Abrahams, J. Albertsson, C. Svensson, and J. Ravez, Acta Cryst. B **46**, 497 (1990); J. Ravez, V. Andriamamplarina, A. Simon, J. Grannec, and S. C. Abrahams, J. Appl. Phys. **70**, 1331 (1991).

[7] S. Arquis-Canouet, J. Ravez, and S. C. Abrahams, J. Appl. Cryst. **19**, 374 (1986).

[8] P. W. Anderson and P. R. Weiss, Rev. Mod. Phys. **25**, 269 (1953).

[9] N. Samarth and J. K. Furdyna, Phys. Rev. B **37**, 9227 (1988).

[10] D. L. Huber, Phys. Rev. B **31**, 4420 (1985).

[11] R. Blinc, M. Kosec, J. Holc, Z. Trontelj, Z. Jaglicic, and N. Dalal, Ferroelectrics **349**, 16 (2007).